MASS TIMBER FRAMES WITH TIMBER BUCKLING RESTRAINED BRACES

E. Williamson[1], C. Pantelides[2], H.-E. Blomgren[3] & D. Rammer[4]

[1] University of Utah, Salt Lake City, USA, emily.diedrich@utah.edu

[2] University of Utah, Salt Lake City, USA, c.pantelides@utah.edu

[3] Timberlab, Portland, USA, HansErik.Blomgren@timberlab.com

[4] Forest Products Laboratory, Madison, USA, douglas.r.rammer@usda.gov

Abstract*: A timber lateral force resisting system (LFRS) with timber buckling-restrained braces (TBRB) is proposed to improve the seismic performance of timber buildings. Using a similar design approach for conventional buckling-restrained braced frames (BRBF) and established design methods for timber connections, a timber buckling-restrained braced frame (TBRBF) was designed and tested under a series of quasi-static cyclic loading protocols. During the tests, the level of axial load applied to the column was varied to simulate gravity loads. Additionally, some of the tests included an out-of-plane displacement imposed on the upper east connection of the frame. The results of these tests show that the TBRBF is able to achieve 1.5 times the requirement for the cumulative inelastic displacement (CID) set by AISC for conventional BRBs. The TBRBFs were able to reach approximately 3.0% story drift before TBRB failure due to splitting of the casing. To improve the performance of the TBRB, some of the tests included a TBRB which was enhanced with carbon fiber wrap at the two ends of the casing. This enhancement increased the story drift capacity to 4.5% and changed the failure mode of the TBRB from splitting of the MPP casing along its length to fracture of the steel core. Finally, the bare frame was tested on its own to provide improved understanding of the performance of the subassembly. The results of the entire experimental program suggest that the TBRBF behaves as a dual system and is well-suited as a LFRS for timber buildings in seismic regions.*

1. Introduction

Recently, mass timber buildings have increased in popularity due to their sustainable characteristics, architectural appeal, reduced weight, and ease of construction. The development of engineered timber products such as cross laminated timber (CLT) and laminated veneer lumber (LVL) have allowed engineers to take advantage of the high strength-to-weight ratio of mass timber. New adaptations of CLT and LVL known as mass ply panel (MPP) and mass ply lam (MPL) provide additional benefits like dimensional stability and self-reinforcing by manufacturing members which consist of multiple 25.4 mm (1-in.) lamina. The 25.4 mm (1-in.) lamina are made of 3 mm (1/8-in.) layers with varying cross-grain directions to achieve a desired elastic modulus for the section (APA 2021). There are currently no ductile timber frame lateral force resisting systems (LFRS) defined in building codes, so projects often have to be a hybrid of structural systems with timber gravity systems and a reinforced concrete or structural steel LFRS. The development of a ductile timber frame LFRS will help expand the use of mass timber in new construction buildings.

Conventional buckling restrained braces (BRB), which have a steel tube filled with mortar or concrete restraining element and a de-bonded steel yielding core, are a popular choice for structural steel buildings because they have been proven to provide a ductile response and reliable energy dissipation (Black et al. 2002; Fahnestock et al. 2007; Palmer et al. 2013; Wu et al. 2014; Xu and Pantelides 2017). Researchers are exploring the use of conventional BRB diagonal members with timber beam and columns frame elements to provide a ductile LFRS (Dong et al. 2020). Separately, researchers have used the same design principles for conventional BRBs to develop a mass timber BRB (TBRB) by testing a 3.7 m (12 ft) long BRB with an MPP casing (Murphy et al. 2021). The TBRBs discussed in Murphy et al. (2021) achieved a maximum strain of 3.9% and reached cumulative inelastic deformations ranging from 2.4 to 7.8 times the AISC 341 minimum requirement for conventional BRBs (AISC 2016); the results of these component tests indicate that the TBRB could be an effective solution for a ductile timber frame, but further testing is required to confirm these results. Additional TBRB studies have been completed which show how TBRBs perform with glulam blocks and steel plates as the restraining element (Takeuchi et al. 2022), or with carbon fiber wrap holding the assembly together in place of bolts (Song et al. 2022).

This paper presents the results of an experimental study in which a series of quasi-static cyclic tests was completed on a 2/3-scale experimental timber buckling restrained brace frame (TBRBF). In this testing series, three TBRBs were tested in the same timber frame according to the loading protocol defined by AISC 341 for the qualification of conventional BRBs. Moreover, two of the tests included carbon fiber reinforced polymer (CFRP) wrap at the two ends of the MPP casing to improve the tensile strength of the timber casing and allow for higher strains in the brace.

2. Timber Frame Design

A schematic of the 2/3-scale experimental frame can be seen in Figure 1. The beam span was 3.05 m (10 ft) and the story height of the frame was 2.29 m (7 ft-6 in.) due to the limitations of the testing facility. The column and beam members had a cross-section of 389 mm (15-5/16 in.) by 381 mm (15 in.) and were made of F16 MPL (APA 2021), which has a modulus of elasticity of 11 GPa (1600 ksi). The experimental frame was designed to be an upper-story frame with a single-diagonal (zig-zag) configuration.

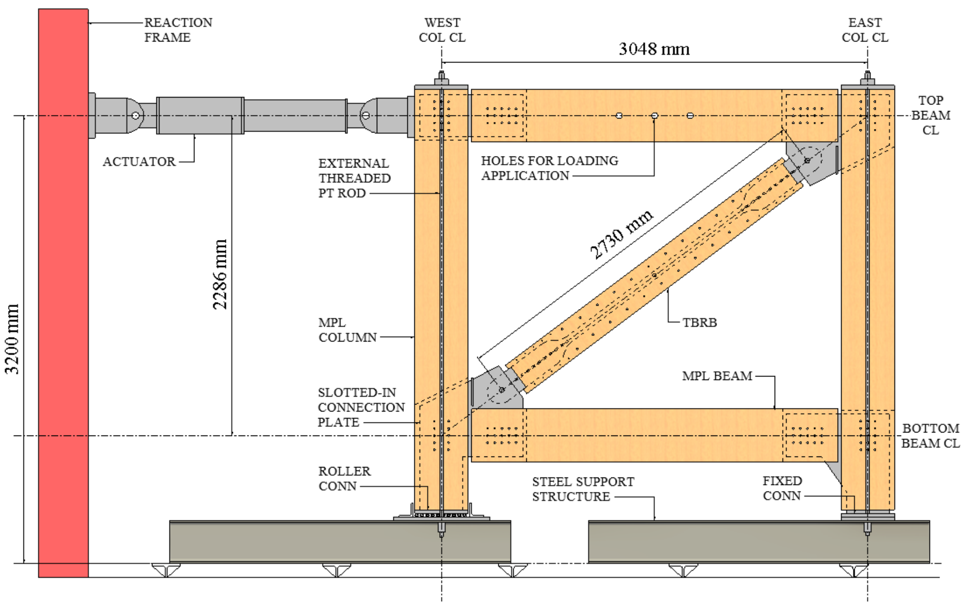

Figure 1: Experimental configuration for TBRBF.

2.1. TBRB Design

Similar design principles to the design of conventional BRBs were adopted for the design of the TBRBs tested during this study. The TBRB was specified to have a tensile yield strength of 178 kN (40 kip). To achieve the yield strength, the steel yielding core was specified to have a yield strength of 276 MPa (40 ksi) and a cross-sectional area of 645 mm^2 (1 in^2.). The restraining elements in the TBRB are the MPP blocks, which are placed on either side of the steel core and bolted together, as shown in Figure 2. The MPP blocks were 254 mm (10 in.) wide by 152 mm (6 in.) deep by 2426 mm (95.5 in.) long and were made of the F10 MPP material layup

(APA 2021), which has and elastic modulus of 6206 MPa (900 ksi). In addition to the MPP blocks, a hardwood spacer was placed on either side of the steel core to prevent it from buckling about its strong axis.

During a previously completed set of TBRBF tests, the common failure mode of the TBRB was splitting of the MPP casing along the glue lines of the LVL layers (Williamson et al. 2023a). CFRP wrap was used in the present testing series in an attempt to mitigate this failure mode. A single layer of CFRP wrap, shown in Figure 2(b) was used at the ends of the TBRB casing to provide confinement and additional tensile strength to the perpendicular to grain direction. The CFRP wrap was designed by estimating the bulging forces imposed on the casing by the weak-axis buckling of the steel yielding core. Equations (1) through (5), as presented by Takeuchi et al. (2022), were used to determine the bulging force, $P_{d,w}$.

$$P_{d,w} = \frac{4N_{cu}(2s_{rw}+\nu_p t_c \varepsilon_t)}{l_{pw} - 4N_{cu}/K_r} \tag{1}$$

N_{cu} is the maximum core compression force; s_{rw} is the weak-axis gap between the core and the MPP casing; l_{pw} is the weak-axis wavelength estimated to be approximately from 9 to 11 times t_c (Wu et al. 2014; Murphy et al. 2021); t_c is the thickness of the steel core; and K_r is the restrainer stiffness, defined in Eqs. (2-5). The tensile strain, ε_t, is the maximum strain expected in the TBRB steel core. For the design of the CFRP wrap, ε_t was assumed to be equal to 2.0% and N_{cu} was assumed to be 267 kN (60 kips) based on the maximum strains and tensile forces achieved by the TBRBs in the testing series performed by Williamson et al. (2023a).

$$K_r = \frac{1}{1/K_w + 1/K_b} \tag{2}$$

$$K_b = \frac{E_b A_{eff}}{D_r/2} \tag{3}$$

$$K_w = \frac{E_w l_{pw} B_r}{D_{rh}} \tag{4}$$

$$A_{eff} = 2 \times \frac{\pi d^2}{4}\left(\frac{l_{pw}}{l_b}\right) \tag{5}$$

where K_b is the stiffness of the bolt; K_w is the stiffness of the wood; E_b and E_w are the elastic moduli of the bolt and MPP, respectively; D_r is the depth of the TBRB assembly; B_r is the width of the restrainer; D_{rh} is the depth of one MPP casing block; A_{eff} is the effective area of the bolts; and l_b is the spacing of the bolts.

Once the bulging force was determined, the number of required layers for the CFRP wrap was determined using the following equation:

$$n = \frac{P_{d,w}}{2F_t w_f t_f} \tag{6}$$

where n is the number of required layers; F_t is the design tensile stress of the CFRP composite; w_f is the width of the CFRP wrap; and t_f is the thickness of a single layer of the CFRP wrap. In this study, the design tensile stress of the CFRP composite was 1248 MPa (181 ksi); the width of the CFRP wrap was 635 mm (25 in.); and the thickness of one layer of CFRP wrap was 1 mm (0.04 in.).

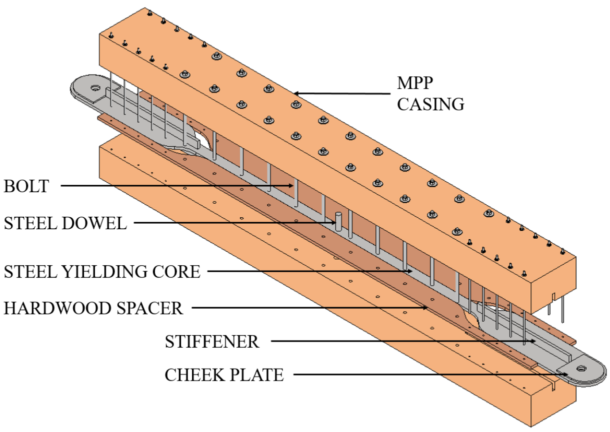

(a)

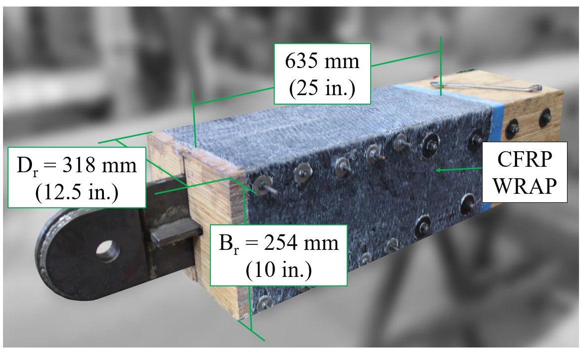

(b)

Figure 2: TBRB assembly (a) original design; (b) with CFRP wrap enhancement.

To determine the expected strength of the TBRB for the design of the elastic elements in the frame, a strain hardening factor, ω, of 1.45 and a compression adjustment factor, β, of 1.25 (Murphy et al. 2021) were used in equations (7) and (8):

$$T_{max} = \omega\, R_y F_y A_{sc} \tag{7}$$

$$C_{max} = \beta\, \omega\, R_y F_y A_{sc} \tag{8}$$

where T_{max} and C_{max} are the maximum expected brace forces in tension and compression, respectively; R_y is the ratio of expected to specified yield stress; F_y is the steel core specified yield stress; and A_{sc} is the cross-sectional area of the yielding portion of the steel core. For the design discussed in this paper, R_y was selected to be equal to 1.0 because the actual yield strength of the core was determined from a series of coupon tests.

2.2. Connection Design

The beam-column connections are an important design consideration for the TBRBF because they need to be able to withstand the forces from the TBRB without experiencing extensive damage. The connections in this frame were designed for the expected forces of the 178 kN (40 kip) TBRB as described in the previous section. An example of one of the beam-column-brace connections is shown in Figure 3(a). These connections were designed according to the equations defined by the National Design Specification for Wood Construction (AWC 2018a), NDS technical report (AWC 2018b), and an equivalent model for connections with multiple slotted-in steel plates (Fan et al. 2011). The geometry of the connection was selected to ensure that the design was governed by yield mode IV, a ductile yield mode for this type of connection.

The design resulted in a connection with fifteen 13 mm (1/2 in.) smooth mild steel dowels in the beam and the column. Two 13 mm (1/2 in.) steel plates with a specified yield stress of 276 MPa (40 ksi) were slotted in to the timber members to connect the beams and columns, while maintaining a 25.4 mm (1 in.) gap to allow for non-binding rotations. In the locations where the TBRB framed into the beam-column joint, the steel connecting plates were extended beyond the timber members to form gusset plates. The gusset plates were reinforced with a stiffener and cheek plates, and the end of the TBRB core was placed between the gusset plates and connected with a pin, as shown in Figure 3(b).

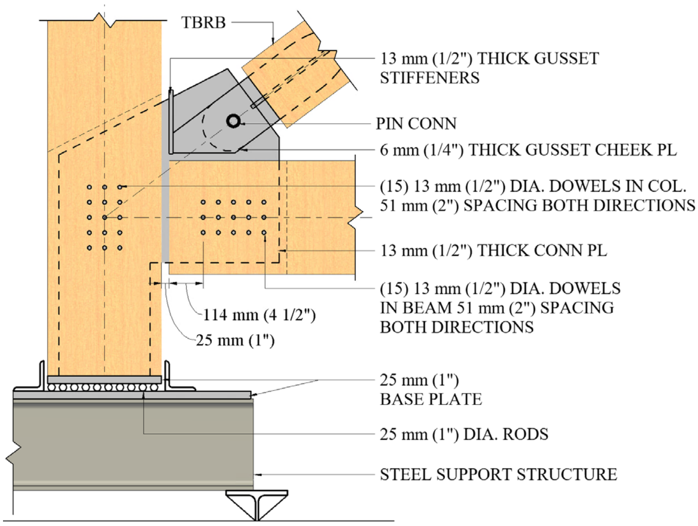

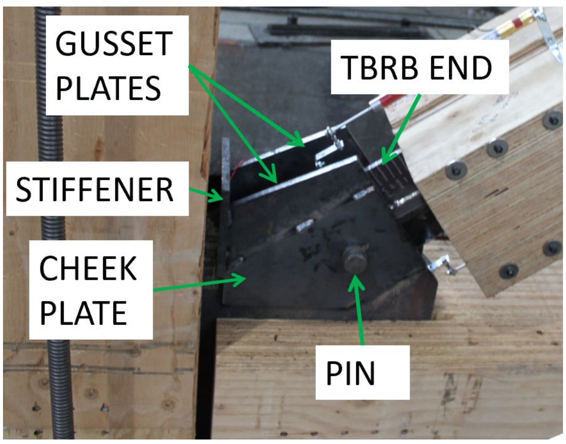

(a) (b)

Figure 3: Beam-column connection with TBRB.

A series of connection tests were completed before the TBRBF tests (Williamson et al. 2023b) in order to better understand the design approach for the connections as well as the bending moment-rotation capacity relationship and potential failure modes. The connection tests showed that the bending moment was approximately proportional to the number of dowels in the beam; moreover, the connections achieved a maximum 0.11 radians of rotation without visible external damage to the frame. Upon completion of the connection tests, the connections were dissected and yielding of the dowels was observed, which suggested that the connection behaved in a yield mode IV failure as designed. The results of the previously completed connection tests suggested that the design approach adopted for the TBRBF connections would allow the TBRB to provide ductile response of the frame, while the connections remained mostly elastic.

2.3. Frame Supports and Loading Application

To best simulate the performance of a frame in an upper story of a building and observe more realistic frame action, the columns were extended below the bottom beam and connected to the steel support structure in the strong floor. The west column base was designed to be a roller connection to drag the force from the TBRB through the bottom beam similar to how a single-brace configuration would bring the lateral force down through a frame. On the east side, the column base was designed as a fixed connection in which all of the horizontal force was transferred to the strong floor. Out-of-plane movement of the TBRBF was restrained using high-strength steel bars, which spanned from the strong floor to the top of the reaction frame, near the front and back of the frame.

Gravity loads in the columns were simulated by applying axial forces to both columns through additional external threaded rods that were post-tensioned so that each column had 120 kN (27 kips) applied to it. To apply the axial load to the columns, two post-tensioned threaded rods were connected to each column by spanning the rods between two 25.4 mm (1 in.) thick plates, which extended north and south beyond the face of the columns. Finally, the horizontal load was applied by the actuator at the center of the top beam with channels, which were extended from the actuator and were connected to the beam, as shown in Fig. 1.

3. Experimental Program

3.1. Instrumentation

String pots were attached to the mid-depth of the top and bottom beams so that the story drift ratio of the frame could be calculated by subtracting the bottom displacement from the top displacement. Linear variable displacement transducers (LVDTs) were attached to the ends of the TBRB to monitor the strain of the steel yielding core throughout the loading protocol. They were also placed on the face of the east connections to monitor the connection rotation during testing. Finally, strain gages were placed in the center of the gusset plates parallel to the line of force from the TBRB.

3.2. Loading Protocol

The loading protocol defined by AISC 341 (AISC 2016) for the qualification of conventional BRBs was adopted as the loading protocol for this testing series. It is a displacement-controlled loading protocol where two cycles are completed at each of the first five steps. The protocol starts with two cycles at the displacement corresponding to the yield displacement of the BRB. Then it moves to 0.5% of the design story drift and increases by 0.5% of the design story drift until reaching twice the design story drift. Following the completion of the first five steps, the researcher can decide how to proceed with the remainder of the loading protocol until BRB failure. In this testing series a fatigue loading protocol (Figure 4a) and an incremental displacement protocol (Figure 4b) were adopted. In the fatigue loading protocol, fifty cycles were repeated at the 1.5% story drift ratio before the displacement was increased by increments of 0.5% of the design story drift after two cycles at each new displacement. During the incremental displacement protocol, the maximum displacement was increased by 0.5% of the design story drift at every other cycle.

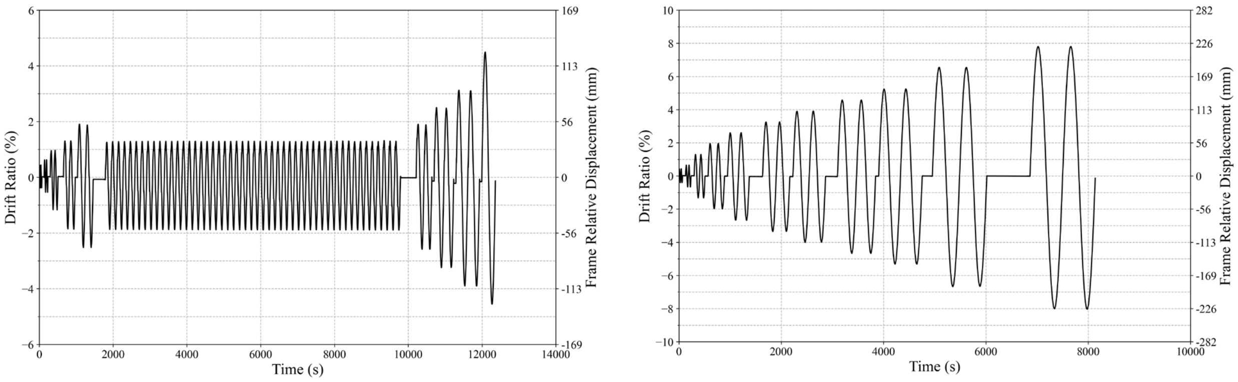

(a) (b)

Figure 4: Loading protocol for TBRB frame tests: (a) fatigue; (b) incremental displacement.

The testing program is summarized in Table 1. Three TBRBF tests were completed using the same timber frame and a new TBRB for each test: one with the original TBRB casing design and two with a TBRB with the CFRP wrap at the two ends of the casing. The test with the original TBRB design and one test with the CFRP followed the fatigue loading protocol while the second test with the TBRB and CFRP wrap followed the incremental displacement loading protocol. Additionally, the timber bare frame was tested on its own at the end of the testing series.

Table 1.Test Matrix.

Test Name	Loading Protocol	TBRB Type
TBRB1	Fatigue	MPP casing only
TBRB2	Incremental Displacement	MPP casing with CFRP wrap at ends
TBRB3	Fatigue	MPP casing with CFRP wrap at ends
Bare Frame	Incremental Displacement	None

4. Experimental Results

4.1. Hysteretic Response

The force versus story drift ratio hysteresis can be seen in Figure 5. For the incremental displacement protocol, Test TBRB2 (Figure 5(a)) achieved a maximum story drift ratio of 3.6% after the steel yielding core fractured in tension. The steel yielding core in test TBRB2 also experienced a second core fracture when the TBRB returned to compression. The bare frame (Figure 5(a)) achieved a maximum story drift ratio of 8.0% without experiencing a loss in strength; the test was terminated after the completion of the 8.0% cycles because the stroke of the actuator had reached its maximum. For the fatigue protocol, Test TBRB1 (Figure 5(b)) reached a maximum story drift ratio of 3.1% when the TBRB failed during the compression phase of the cycle when the MPP casing began to split. TBRB3 (Figure 5(b)) experienced tensile fracture of the steel yielding core and reached a maximum story drift ratio of 4.5%.

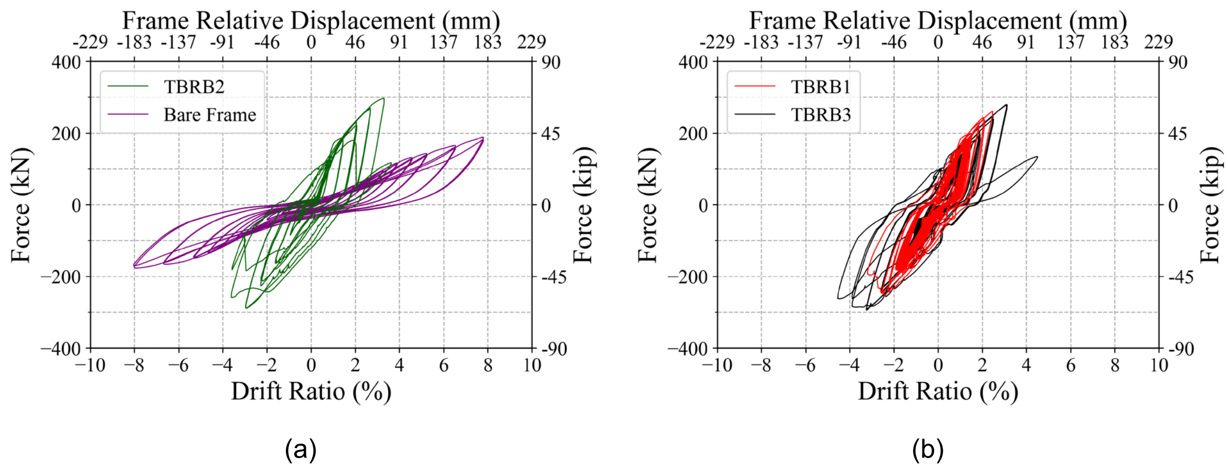

Figure 5: Hysteresis curves (a) tests with incremental displacement protocol; (b) tests with fatigue protocol.

The hysteresis loops of the TBRBF tests experienced minimal pinching compared to the hysteresis of the Bare Frame test. This is because the TBRB provides higher stiffness and strength to the subassembly than the beam-column connections, so the TBRBF was impacted less by the slip of the system caused by the movement of the dowels within the holes. Each TBRB test achieved similar maximum forces in the positive and negative directions. Additionally, Figure 5(a) helps illustrate the contribution of the TBRB and the bare frame to the subassembly. When the core in TBRB2 fractures in tension, the load drops to approximately the load resisted by the bare frame at the same story drift ratio during the Bare Frame test.

The cumulative hysteretic energy is plotted for each test in Figure 6(a). Tests TBRB1 and TBRB3 show higher dissipated energy than the other two tests because TBRB1 and TBRB3 were subjected to the fatigue loading protocol. It is likely that TBRB1 dissipated more energy during the repeated fifty cycles than TBRB3 because the connections in the frame were untested during the first test and therefore had higher stiffness than the subsequent tests in which the timber around the dowels had already begun to be crushed during the previous tests. After completing 14 cycles of the incremental displacement loading protocol, TBRB2 dissipates approximately 5 times more hysteretic energy than the bare frame after the same number of cycles.

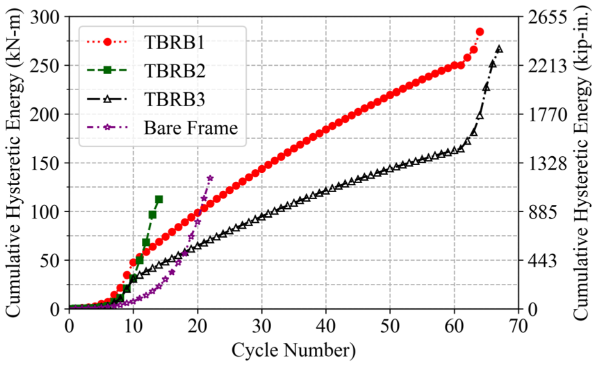

(a)

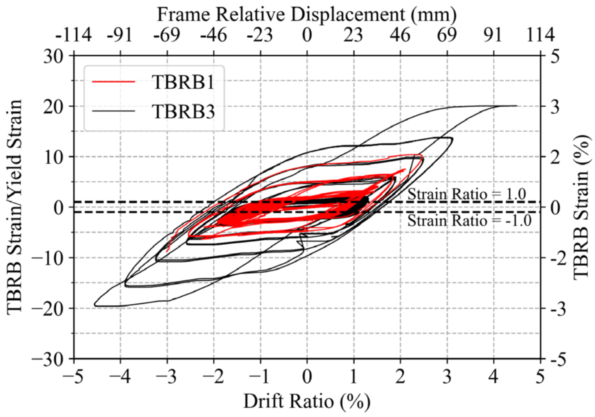

(b)

Figure 6: Experimental results: (a) cumulative hysteretic energy; (b) TBRB core strain.

The average strain of the TBRB during the tests was calculated by summing the displacement measured by the LVDTs at either end of the MPP casing and divided by the yielding length of the core, 1556 mm (61.25 in.). The TBRBs with the CFRP wrap at the two ends of the casing reached twice the tensile strain achieved by the TBRB without the CFRP wrap. The TBRB without the CFRP wrap tested in the present research reached strains that were slightly less than the strains measured in the TBRBs tested by Murphy et al. (2021). The lower strains could be a result of the shorter yielding cores of the present TBRBs or the difference in loading conditions. In Murphy's tests, the load was applied concentrically with the core while the load in the present tests was likely applied to the core in an eccentric manner due to the more complicated testing configuration within the frames. In addition, the pins connecting the TBRB to the gusset plates likely had some friction, which could've introduced additional moments to the end of the TBRB that were not present in the component tests (Murphy et al. 2021). Further TBRB testing is planned to better understand the impact of the end connections on the performance of the TBRBs.

4.2. **Damage observations**

The failure mode of test TBRB1 was splitting of the MPP casing along the length of the casing and in between lamina, as shown in Figure 7. The failure mode of tests TBRB2 and TBRB3 was fracture of the steel core while the casing remained intact, as shown in Fig. 8 for test TBRB2.The steel yielding cores for each of the TBRBF tests are shown in Figure 9(a). Weak axis buckling is observed in all three steel cores. TBRB1, with the original casing design, shows multiple distinct waves along the entire yielding region. Small waves can also be seen along the length of the yielding region in TBRB2 and TBRB3; however, the wave at the end of the yielding region is significantly more pronounced than the other waves. Additionally, TBRB2 and TBRB3 experienced fracture of the steel yielding core near the end of the yielding region.

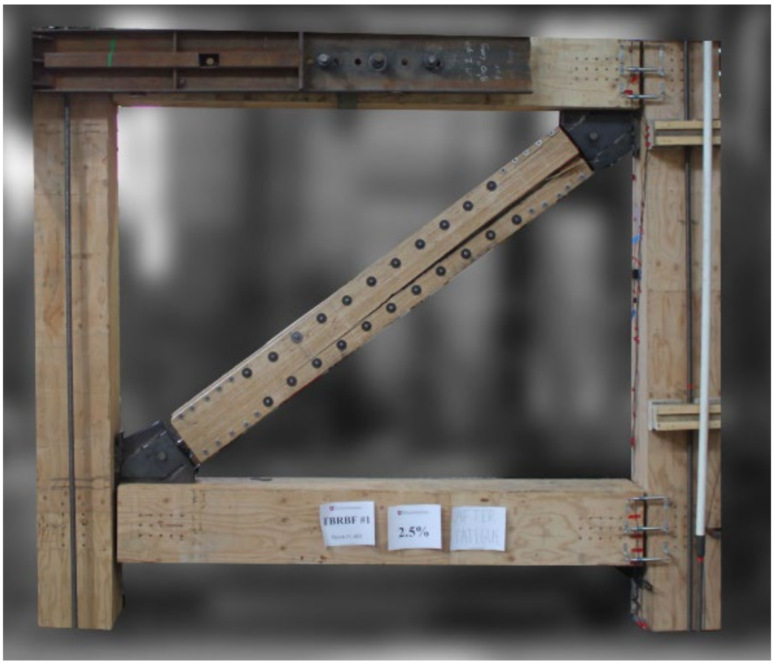

Figure 7: TBRBF after the completion of test TBRB1.

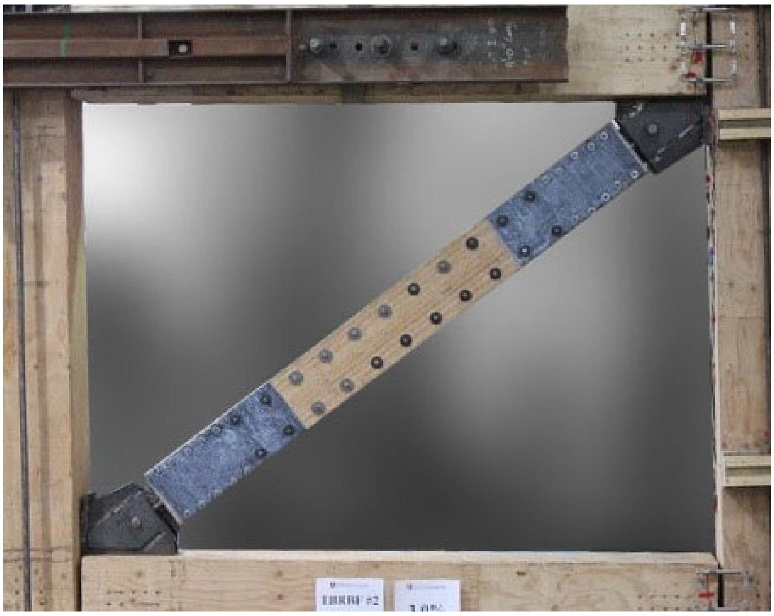

Figure 8: TBRBF after the completion of test TBRB2.

The weak axis buckling of the steel yielding core caused the MPP casing to deform, similar to what is shown in Figure 9(b). For the TBRB with no CFRP wrap (TBRB1) the indentations into the casing were minor because the casing began to split apart due to the bulging forces from the steel yielding core. The CFRP wrap included in the other two TBRBs helped prevent splitting of the casing, so the deformation in the MPP casing was more significant.

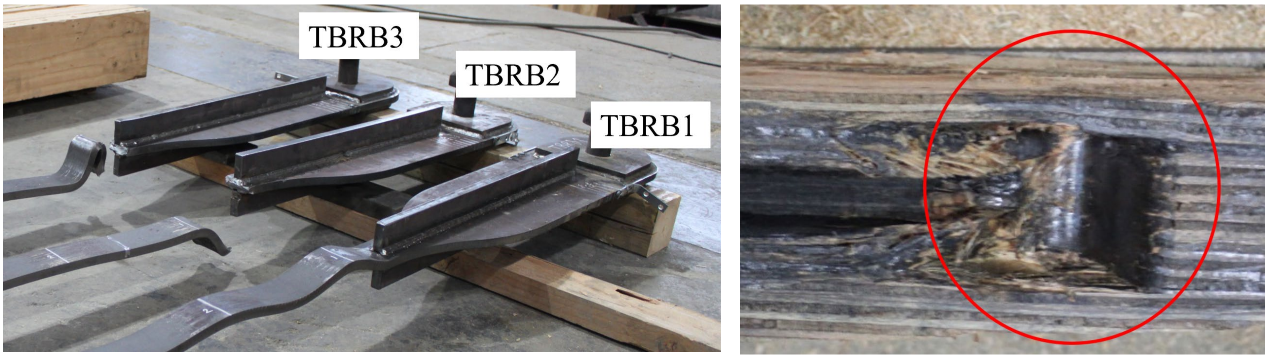

(a) (b)

Figure 9: TBRB failure modes (a) steel yielding cores; (b) MPP casing.

Throughout the entire testing series, no visible external damage of the mass timber frame such as timber splitting or crushing was observed. Following the conclusion of the bare frame test, the connections were dissected to observe the state of the dowels inside the connection. Some minor damage was observed in the corner dowels of the connections such as dowel bending and a reduced diameter at the steel plate interface. Finally, no damage or yielding of the gusset plates occurred during this testing series.

5. Conclusions

This paper discusses the design and results of three TBRBF quasi-static cyclic loading tests. One of the TBRBs tested in this series followed the original TBRB design while two of the TBRBs included a CFRP wrap at the two ends of the MPP casing to help restrain the casing and prevent premature splitting observed in the original TBRB design. Based on the results of the tests the following conclusions can be made:

- The CFRP wrap changes the failure mode from splitting of the MPP to fracture of the steel core; however, the MPP casing enhanced with the CFRP wrap at the two TBRB ends still experiences extensive damage due to indentation of the casing caused by the higher amplitude buckling of the steel yielding core which occurred during the tests.
- Preventing the splitting of the MPP casing with the CFRP wrap allowed the maximum story drift ratio to increase from 3.1% to 4.5%, and the maximum tensile strain of the steel core to reach 20 times the yield strain for the fatigue loading protocol.
- The TBRBF subassembly was able to dissipate five times the hysteretic energy dissipated by the bare frame after completing the same number of cycles during the incremental displacement loading protocol.
- The TBRBF resists approximately three times the amount of lateral force than the bare frame at the same story drift ratio.
- The connections in the frame experienced minimal damage even after three TBRBF tests and a bare frame test, which reached 8.0% story drift. This suggests that even if the TBRB core were to fracture during a large seismic event, the bare timber frame would likely be able to survive and a new TBRB could be installed after the earthquake.

6. References

AISC (American Institute of Steel Construction). 2016. *Seismic Provisions for Structural Steel Buildings*. ANSI/AISC 341-16, Chicago, IL.

APA (Engineered Wood Association). (2021). Freres Mass Ply Panels (MPP), and Mass Ply Lam (MPL) Beams and Columns. Freres Lumber Co., Inc. PR-L325. Tacoma, WA.

AWC (American Wood Council). 2018a. National Design Specification for Wood Construction. Leesburg, VA.

AWC (American Wood Council). 2018b. Technical Report 12: General Dowel Equations for Calculating Lateral Connection Values with Appendix A. Leesburg, VA.

Black CJ, Makris N, Aiken ID. (2004). Component testing, seismic evaluation and characterization of BRBs. *J. Struct. Eng*. 130 (6):880–94. https://doi.org/10.1061/(ASCE)0733-9445(2004)130:6(880).

Dong W., Li M., Lee C., MacRae G., and Abu A. (2020). Experimental testing of full-scale glulam frames with buckling restrained braces. *Engineering Structures* 222. https://doi.org/10.1016/j.engstruct.2020.111081.

Fahnestock LA, Sause R, Ricles JM. (2007). Seismic response and performance of buckling-restrained braced frames. *J. Struct. Eng*. 133(9):1195–204. https://doi.org/10.1061/(ASCE)0733-9445(2007)133:9(1195).

Fan X., Zhang S. and Qu W. 2011. “Load-carrying behaviour of dowel-type timber connections with slotted-in steel plates.” *Applied Mechanics and Materials*, 94-96(8): 43-47.

Murphy C., Pantelides C.P., Blomgren H., and Rammer D. (2021). Development of Timber Buckling Restrained Brace for Mass Timber-Braced Frames. *J. Struct. Eng*. 147(5). https://doi.org/10.1061/(ASCE)ST.1943-541X.0002996.

Palmer K.D., Roeder C.W., Lehman D.E., Okazaki T. and Shield S. 2013. “Experimental performance of steel braced frames subjected to bidirectional loading.” *J. Struct. Eng.* 139(8): 1274-1284. https://doi.org/10.1061/(ASCE)ST.1943-541X.0000624.

Song X.-B., Wu Y.-J., Jiang H.-Y. and Chen T. (2022). Lateral performance of glulam timber frames with CFRP confined timber-steel buckling-restrained bracings. *J. Struct. Eng*. 148(3). https://doi.org/10.1061/(ASCE)ST.1943-541X.0003273.

Takeuchi T., Terazawa Y., Komuro S., Kurata T. and Sitler B. (2022). Performance and failure modes of mass timber buckling-restrained braces under cyclic loading. *Engineering Structures* 266. https://doi.org/10.1016/j.engstruct.2022.114462

Williamson E., Pantelides C. P., Blomgren H.-E. and Rammer D. 2023a. “Design and cyclic experiments of a mass timber frame with a timber buckling restrained brace.” *J. Struct. Eng.* 149(10): 04023131. https://doi.org/10.1061/JSENDH/STENG-12363.

Williamson E., Pantelides C. P., Blomgren H.-E. and Rammer D. 2023b. “Performance of beam-column connections with mass ply lam and steel dowels under cyclic loads.” *J. Structural Engineering*, 149(6), 04023057, 10.1061/JSENDH.STENG-11569.

Wu A.-C., Lin P.-C., and Tsai K.-C. (2014). High-mode buckling responses of buckling-restrained brace core plates. *Earthquake Engineering Structural Dynamics* 43(3): 375–393. https://doi.org/10.1002/eqe.2349.

Xu, W., and Pantelides, C.P. (2017). Strong-axis and weak-axis buckling and local bulging of buckling-restrained braces with prismatic core plates. *Engineering Structures* 153: 279-289. https://doi.org/10.1016/j.engstruct.2017.10.017.